Eur. Phys. J. B **37**, 149–162 (2004)
DOI: 10.1140/epjb/e2004-00041-1

THE EUROPEAN PHYSICAL JOURNAL B

Quantum well states in thin (110)-oriented Au films and k-space symmetry

E. Hüger[1] and K. Osuch[2,a]

[1] Institute of Physics and Physical Technology, Technische Universität Clausthal, 38678 Clausthal-Zellerfeld, Germany
[2] Department of Physics, University of South Africa, P.O. Box 392, Pretoria 0003, South Africa
and
Institute of Mathematics and Physics, University of Podlasie, 3-go Maja 54, 08-110 Siedlce, Poland

Received 10 September 2002 / Received in final form 1st December 2003
Published online 15 March 2004 –

Abstract. We present electron diffraction and electron photoemission results for thin Au films grown on Nb(100) in a hexagonal close-packed stacking sequence, which is unusual for Au. Strong *d*-band [48] quantum size effects occur in photo-electron spectroscopy from 5–26 monolayer thick ($11\bar{2}0$) oriented Au films whose confined direction ([11.0]) is not perpendicular to any face of the bulk Brillouin zone. Also in this case, the energetics of the quantum well states can be explained by a discretisation of the bulk band structure corresponding to the quantum well. However, the bulk states corresponding to the quantum well states do not lie in the confined direction of the first bulk Brillouin zone, contrary to what is required by the quantum well. This can be remedied by the construction of a layer symmetry adapted Brillouin zone, which is consistent with the symmetry of the quantum well but different from the bulk one. We subsequently determine, for the first time, the $k_{\parallel}$ periodicity of the quantum well states from their measured $E(k_{\parallel})$. This periodicity proves to be consistent with the newly introduced Brillouin zone.

PACS. 73.21.-b Electron states and collective excitations in multilayers, quantum wells, mesoscopic, and nanoscale systems – 82.80.Pv Electron spectroscopy (X-ray photoelectron (XPS), Auger electron spectroscopy (AES), etc.) – 71.15.Mb Density functional theory, local density approximation, gradient and other corrections – 71.20.Gj Other metals and alloys

1 Introduction

A standard exercise in elementary quantum mechanics is to describe the properties of an electron confined in a potential well. A potential well can be experimentally realised in a thin film, which confines the motion of the electrons in the direction normal to its surface [1–5]. The surface barrier on the vacuum side of the film and a band gap that prohibits wave propagation across the interface cause electron confinement. As a result, states at discrete energies with quantised wave vectors appear concurring with the standard quantisation condition for a potential well:

$$k_{\perp}(E) \cdot t + \Phi(E) = n\pi \qquad (1)$$

where $k_{\perp}$ is the component of a wave vector in the confined direction, t is the film thickness, n is an integer specifying the number of halve wavelengths which fit into the well and $\Phi(E)$ is the phase shift at the two film boundaries [1–4,6–8].

A key complication in the description of the quantum well states (QWS) of a film in comparison to a simple rectangular potential well is the influence of the periodic potential within the well introduced by the individual atomic layers [3]. It can be argued that both Bloch and QWS are exposed to the same lattice potential and, therefore, the QSE energies should be contained in the respective bulk band structures. This has so far been confirmed by all measured QSE energies, which can be explained in terms of the respective bulk band structures. However, it is not clear, whether, in general, QWS energies can be obtained from the band structure given in the conventional bulk Brillouin zone (BZ). The bulk BZ is defined for translational symmetry extending to infinity in all the lattice directions of a bulk crystal and, in general, no translational directions of a crystal are unique (they can be transformed into one another by symmetry operations of the crystal class). On the other hand, the confined direction of a film is unique and no symmetry operations of the system (film) can transform it into another direction in the first Brillouin zone. Thus, the application of the bulk BZ to the description of QWS leads to the following two problems: one concerns the irreducible states in the confined direction and the other – inversion symmetry in that direction. Until now only those QSE were analysed whose confined direction is perpendicular to a face of the bulk BZ. In this particular case almost all the irreducible

[a] e-mail: osuchk@harry.unisa.ac.za

states situated in the confined direction lie in the first bulk BZ. If, however, a general case is considered where the surface normal direction is not perpendicular to any face of the bulk BZ, there always exist irreducible QWS in this direction whose k vectors lie outside of the first bulk BZ. Due to the bulk symmetry, these states can be transformed into the first bulk BZ (which contains all the irreducible states), but not into the confined direction as required by the quantum well problem. The other problem concerns the application of a simple quantum well model to the description of QSE in thin films. Due to inversion symmetry QWS with $-k_\perp$ and $+k_\perp$ always obey the condition $E(-k_\perp) = E(+k_\perp)$. Obviously the same condition is fulfilled by all the $k_\parallel$ values. However, the condition $E(-k_\perp) = E(+k_\perp)$ is not always satisfied in the bulk BZ. For example, if the confined direction is the [111] direction of an fcc crystal (the case of (111) oriented fcc films) all the states with $k_\parallel$ off the $\langle 110\rangle$ direction, do not fulfil this condition. The violation of inversion symmetry by these vectors leads to serious problems in constructing QWS. QWS, being standing waves in the confined direction, can be constructed as linear combinations of two states propagating in opposite directions: $(\psi(-k_\perp))$, $\psi(+k_\perp))$ [7,11] which have to satisfy the requirement $E(-k_\perp) = E(+k_\perp)$. This means, that for (111) oriented fcc films no QWS with $k_\parallel$ off the $\langle 110\rangle$ direction can be constructed out of the states given in the bulk BZ since they do not satisfy the condition $E(-k_\perp) = E(+k_\perp)$. Despite that, QWS in thin (111) oriented Ag and Al films have been experimentally observed for $k_\parallel$ values off the $\langle 110\rangle$ direction [12]. This shows that bulk BZs are not always adequate for the explanation of QWS in thin films, since they do not conform to the symmetry of these systems. In order for QWS to be explained in terms of the respective bulk band structures, the latter must be given in BZs which are consistent with the symmetry of quantum wells.

Agreement between the measured and theoretically predicted periodicities of QWS was achieved by the introduction of two models: the "envelope function model" [6] and the "reduced quantum number model" [7]. These models correlate the measured QWS periodicities (e.g. those observed in photoemission experiments [1–4]) with the respective bulk band structure given in the bulk BZ. The "reduced quantum number model" introduces a reduced quantum number ($\nu = N - n$), where N is the number of monolayers. In the "envelope model" the wave function of a QWS is expanded around the Bloch state at the band edge. This fast-oscillating Bloch state is modulated by a slowly varying envelope function, which guaranties that the boundary conditions are satisfied at the two film boundaries [6]. Consequently, the wave vector $k_\perp$ of the QWS is related to the wave vector $\widetilde{k_\perp}$ of the envelope function by the formula [6] $k_\perp = \pi/d - \widetilde{k_\perp}$, where d is the thickness of one monolayer (ML). An essential assumption on which the model is based requires [9] that $k_\perp \simeq 0$, which means that it can only be applied to QWS whose wave vectors $\widetilde{k_\perp}$ lie close to the band edge. Despite that, QSE have been observed whose k values lie far away from the zone boundary [5]. Some authors [4,8] raised the question whether the envelope function and the reduced quantum number models are only a book keeping trick [8], or whether they have some underlying physical significance [4,8].

In this work we report for the first time QWS whose confined direction is not perpendicular to a face of the bulk BZ. Consequently, the irreducible bulk states corresponding to the QWS lie outside of the first bulk BZ. They can be transformed into the first bulk BZ, but not into the confined directions as required by the quantum well. In order to get them situated in the confined direction inside the first BZ, we have to rearrange the bulk band structure into a BZ different from the bulk one but consistent with the symmetry of the quantum well (film). The introduction of this BZ brings about agreement between the QWS and the bulk band structure without the application of the envelope function or the reduced quantum number model. Since the observed QWS are of d-type [48] and for Au the d bands do not intersect the Fermi energy, we were able to determine, for the first time, from the $E(k_\parallel)$ dependence measured with ARUPS, the $k_\parallel$ periodicity of the QWS. The results confirm the proposed shape of the layer symmetry adapted Brillouin zone (LSA-BZ).

The article is organised as follows. Section 2 gives a brief description of the experimental and computational procedure. Section 3 provides a comprehensive presentation of the experimental and theoretical results. In Section 3.1 we present the normal emission UPS measurements, specifying the condition for the observation of pronounced QSE in Au deposited on Nb(100). In Section 3.2 we analyse the QSE data in order to obtain the $E(k_\perp)$ values of the related QWS. It is shown there that the confined direction (the surface normal direction) is along the [110] crystal axis, which is not perpendicular to any surface of the bulk BZ. In Section 3.3 we demonstrate that agreement between the QWS energies and the bulk band structure given in the bulk BZ can be obtained if the two QSE models [6,7] described in the Introduction are applied. However, the corresponding irreducible Bloch states lie outside of the first bulk BZ, whereas the equivalent states lie inside the bulk BZ, but not in the confined direction as required by the quantum well. This can be remedied by the construction of a layer symmetry adapted Brillouin zone (LSA-BZ), which is consistent with the symmetry of the quantum well but different from the bulk one. Section 3.4 shows, that the $k_\parallel$ periodicity of LSA-BZ can be verified by performing off-normal ARUPS measurements, from which the $E(k_\parallel)$ dependence can be determined. In Section 3.5 we compare the $E(k_\parallel)$ dependence of QWS with that of the corresponding bulk states given in the bulk BZ, and subsequently in LSA-BZ. The last section summarises the results and shows that, in contrast to the bulk BZ, LSA-BZ explains also other k-symmetry properties of QWS.

2 Computational and experimental details

The calculations were performed within the framework of density functional theory (DFT), using the full potential

linearised plane wave (FLAPW) method and the GGA approximation [16] as implemented in the Wien'97 package [17]. First scalar relativistic calculations were carried out and subsequently spin-orbit coupling was included in a second variation step [17]. The calculations were performed at 200 k-points in the irreducible wedge of the Brillouin zone. The optimum lattice constant of hcp Au was determined by minimising the total energy as a function of the lattice constant. Convergence of the self-consistent calculations was assumed when the charge distance defined as $\int |\rho_n(r) - \rho_{n-1}(r)| d^3r$, where ρ is the charge density and n is the iteration number, was smaller then 1×10^{-4}e in three consecutive iterations.

The experiments were performed using a VG-ESCALAB spectrometer, which was connected with a home build chamber equipped with a reflection high-energy electron diffraction (RHEED) apparatus. The base pressure of the chamber (3×10^{-11} mbar) rose to 7×10^{-11} mbar during the metal deposition from water cooled evaporators. The surface quality and growth mode were examined by RHEED, Auger electron spectroscopy (AES) and angle resolved ultraviolet photoelectron spectroscopy (ARUPS). The geometric structure was determined by RHEED and X-ray photoelectron diffraction, the electronic structure with AES, X-ray photoelectron spectroscopy (XPS) and ARUPS. Unpolarised vacuum ultraviolet light from a noble-gas resonance lamp with the photon energy of 21.22 eV (HeI) was used in the experiments. The measurements were made with the energy resolution of the UPS system of 60 meV and the angular acceptance of $\pm 1°$. The polar and azimuthal angles of emission were changed by rotating the sample. Cooling with liquid nitrogen (LN_2) was used to lower the temperature of the sample to 150 K, and heating with electron bombardment to raise it to the melting point.

For epitaxy and other studies it is important to prepare well ordered surfaces with bulk lateral periodicity which remain free of oxygen upon heating after cleaning at low temperatures by sputtering with 1 KeV Ar ions. Yet, on the Nb(100) surface oxygen induces a rearrangement of the surface Nb atoms destroying their bulk lateral periodicity. The removal of O from Nb and Ta surfaces without serious deterioration of the surface perfection has been a major problem in nearly all the studies of these surfaces in the past [18]. The difficulty is due to the high solubility and diffusivity of O in these metals and also to the low vapour pressure of its suboxides. We have found an experimental procedure which suppresses oxygen diffusion to the Nb surface while maintaining the bulk lateral periodicity of Nb(100). This was achieved by depositing on the Nb surface suitable metals, like Pd or Au, after its cleaning by sputtering with 1 keV Ar ions, followed by annealing to elevated temperatures (1200 K to 1600 K). This process lead to a flat Nb(100)-like surface, terminated with one pseudomorphic Pd or Au monolayer, free of contamination (C:Nb, O:Nb AES signal ratio 1:500), with the sought for bulk lateral periodicity of the (100) oriented Nb crystal. This surface was further used as the substrate for our metal epitaxy investigations.

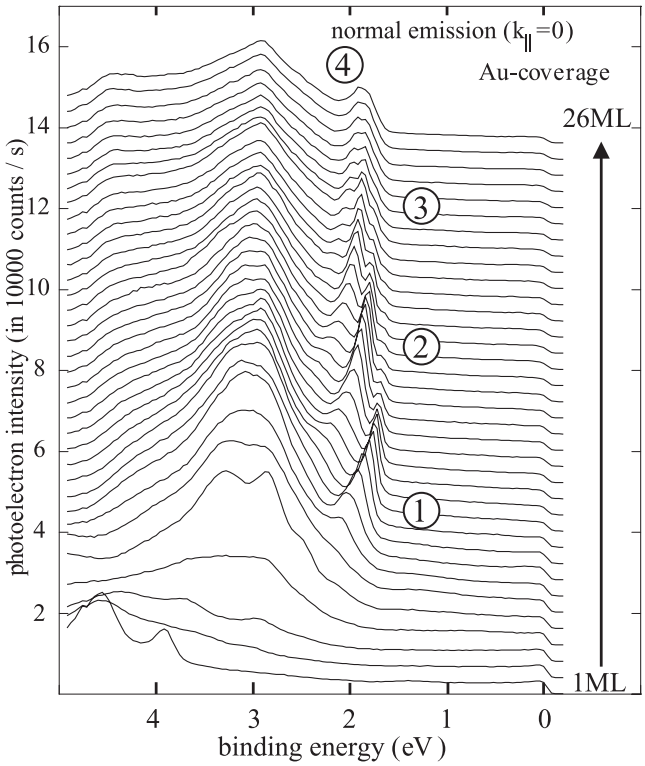

Fig. 1. Normal emission UPS spectra taken in situ at 150 K during the growth of Au on Nb (100).

3 Results and discussion

3.1 Normal emission ARUPS

Figure 1 shows the normal emission UPS spectra recorded during the growth of Au on Nb(100). Noticeably, the energy positions of the minima and maxima of the photoelectric current between 2.3 eV and 1.7 eV change with the thickness of the film varying in the range 5–26 ML. These fluctuations of the current can be explained by the occurrence of QSE which restrict the allowed values of $k_\perp$ of the electrons in the Au film. Concurring with the standard quantisation condition for a potential well given by equation (1), a change of the film thickness (t) is accompanied by a change of $k_\perp$, and, due to the band dispersion, by a change of the energy $E(k_\perp)$, which leads to a shift of the energy position of the UPS peaks. We have investigated in detail the conditions for the appearance of the QSE of Figure 1. To this end we: (i) deposited Au with various deposition rates, (ii) kept the substrate at various temperatures during the Au deposition, (iii) deposited Au on flat or rough substrate surfaces, (iv) changed the atomic periodicity ((1×1) or a reconstructed Nb(100) surface) of the substrate surface before depositing Au there, and (v) changed the chemical composition of the substrate surface maintaining the same (1×1) surface order and Nb periodicity, before starting with Au deposition. We observed, that the pronounced QSE of Figure 1 are not affected by the deposition rates, but occur only if Au is deposited at low temperatures (lower than 200 K) on a Nb(100) surface (1×1)-terminated with a d-band metal. Figures 2a, b

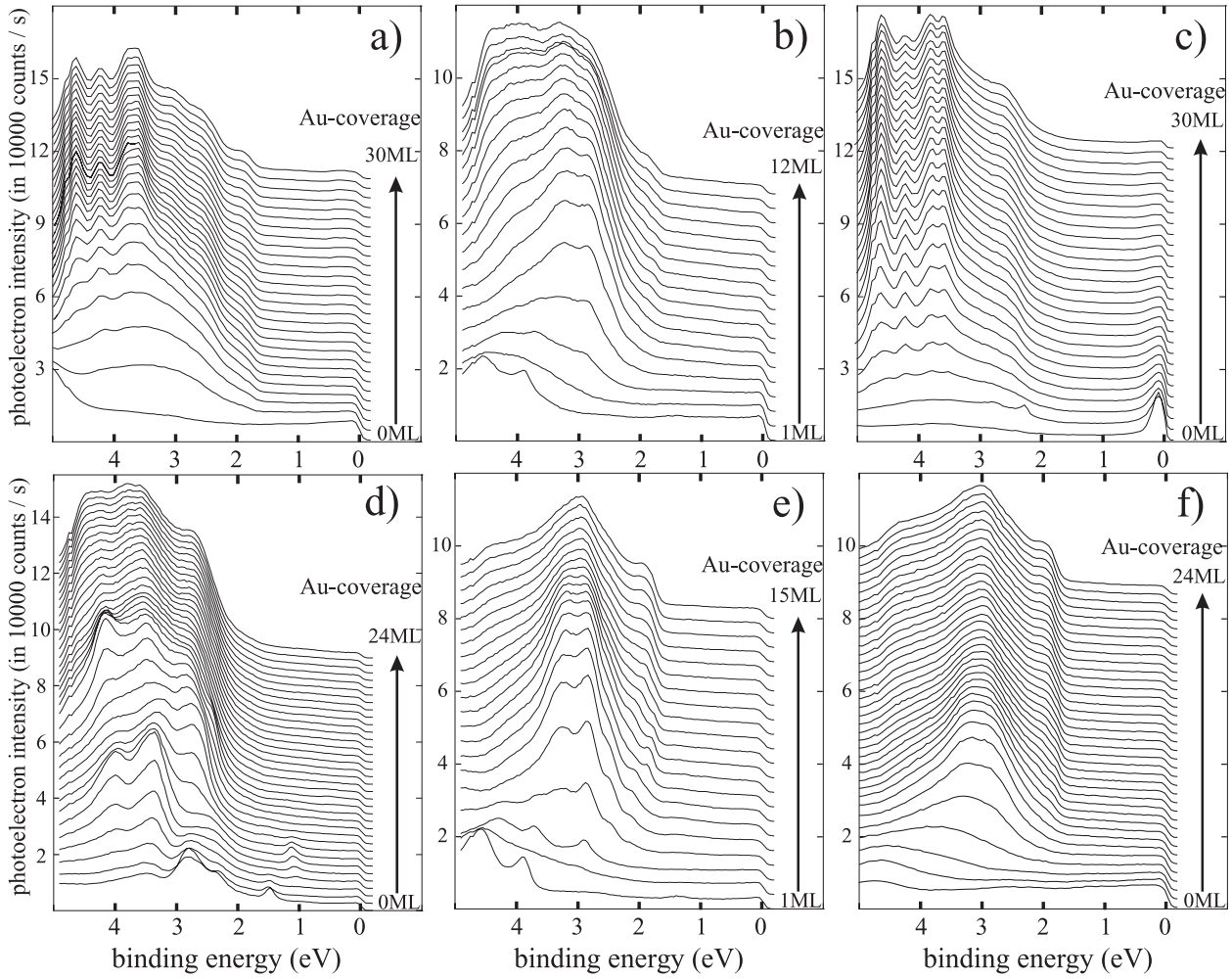

Fig. 2. Normal emission UPS taken in situ during the deposition of Au on various Nb(100) surfaces. a) Au on an oxygen induced p(3 × 1) reconstruction of the Nb(100) surface. b) Au on a flat, Au induced p(4 × 4) reconstruction of the Nb(100) surface. c) Au on a flat, Nb(100) surface (1 × 1)-terminated with S. d) Au on a flat, Nb(100) surface (1 × 1)-terminated with Pd-Al. e) Au on the flat, Nb(100) surface terminated with a pseudomorphic Au monolayer. f) Au on a sputter-rough Nb(100) surface. Except for (e), where the deposition was done at 300 K, in all the other cases it was done at 150 K.

show the in situ measured ARUPS spectra during the deposition of Au on an oxygen induced (3 × 1) reconstruction of the Nb(100) surface (panel (a)) and on an Au induced p(4 × 4) reconstruction of the Nb(100) surface (panel (b)). The p(4 × 4) Au-induced reconstruction of Nb(100) occurred only occasionally, when very thick (more than 100 ML's) Au films had been annealed at temperatures higher than 1400 K. On the both reconstructed surfaces QSE did not occur at any deposition temperature. Figure 2c, d shows the in situ recorded ARUPS spectra during the deposition of Au on a (1 × 1)-S terminated Nb(100) surface (panel (c)) and on a (1 × 1)- Pd-Al terminated Nb(100) surface (panel (d)). The latter surface was obtained by annealing to 900 K a 20 ML thick Al film deposited on a (1 × 1) Pd-terminated Nb(100) surface. RHEED performed on this surface indicates the existence of a (1 × 1) pattern, whereas AES and UPS the presence of Pd and Al on the surface. Panels (c) and (d) of Figure 2 show that although the deposition is made on a flat (1 × 1)-terminated Nb(100) surface kept at a low (150 K) temperature, QSE of the kind shown in Figure 1 do not occur in the film. In all the four presented deposition cases, the UPS spectra (Figs. 2a, b, c, d) are different from that of Figure 1, indicating the growth of Au in orientations different from that related to Figure 1. Finally, Figures 2e, f display the ARUPS spectra recorded in situ during the growth of Au on a flat (1 × 1)-Au terminated Nb(100) surface kept at 300 K (panel (e)) and on a mild sputter-rough Nb(100) surface (panel (d)). They show UPS spectra very similar to those of Figure 1, indicating the same Au film orientation. Indeed, our crystal structure investigation, and especially XPD [23–25], which gives information about the local arrangement of the atoms in real space, shows that the Au films, deposited on a rough Nb(100) surface (Fig. 2d) and on a flat (1 × 1)-Au terminated Nb(100) surface Figures 1, 2e have both the same crystal orientation (the same short range order) independently of the deposition temperature.

Despite that, the QSE emission is not pronounced in Figures 2e, f because the Au films are rough. In the case of the Au growth on a sputter-rough surface the films are always rough giving RHEED [31] transmission patterns, whereas in the Au deposition on the Nb(100) surface kept at 300 K (Fig. 2e) the films begin to be rough after 5 ML of Au have been deposited. The roughness begins exactly at the Au coverage at which the pronounced QSE in Figure 1 occur and explains why the QSE shown in Figures 2e, f are very weak and 'smeared out'. A variation of the number of atomic monolayers in a film leads to a superposition of the emission from QWS occurring in layers of different thickness, thus inhibiting their observation in measurements, such as ours, which average over regions of $\sim$2 mm^2. Therefore, a sharp interface and a narrow height distribution are crucial for the observation of quantum well peaks in the spectra. This means, that QWS can be observed continuously during a deposition if the film grows in a layer-by-layer fashion on a flat substrate surface, like a (1×1)-Pd (not shown here) or -Au terminated Nb(100) surface kept at low temperatures.

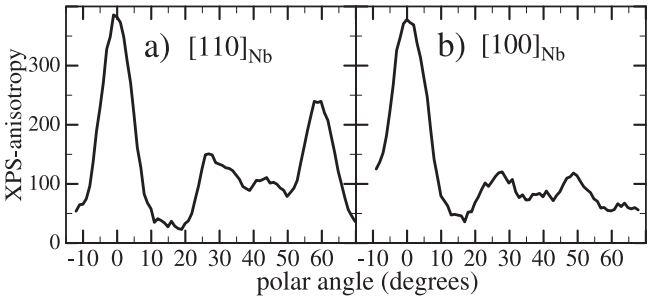

Fig. 3. The polar angle distribution of the background corrected X-ray photoelectron intensity from the Au-4f core-levels of a 14 ML thick Au film deposited at 150 K on the (1×1) Au terminated Nb(100) surface. The polar angle was changed in the plane perpendicular to the surface, aligned along the high symmetry directions $[110]_{\rm Nb}$ (panel (a)) and $[100]_{\rm Nb}$ (panel(b)) of the Nb(100) surface. The surface normal direction corresponds to $\theta = 0°$. The kinetic energy of the Au-4f photoelectrons excited by Al Kα radiation is $\sim$1400 eV. For the background correction the angle distribution of inelastic electrons with the kinetic energy of $\sim$1300 eV was measured. This background emission, which does not show any peaks, was multiplied by a constant factor and then subtracted from the elastic signal.

3.2 Analysis of QSE in normal emission ARUPS

Although ARUPS is the standard method used to determine electronic band structures, which is of fundamental importance for many solid state properties, it has the deficiency of leaving the normal component $k_\perp$ of the final and initial band state unknown. This is so because there is no known relation between the momentum of the detected photo-electron and the normal component $k_\perp$ of the excited or initial band state. This difficulty can be avoided if the normal component $k_\perp$ of the band state is determined independently of the photo-emission process. The following consideration shows how the wave vector of the ground state can be determined on the grounds of QSE. The QWS existing in a film can be viewed as states confined in a potential well of thickness t with finite walls, whose wave length λ fulfils the quantisation condition $\mathrm{n}\cdot\lambda/2 = \mathrm{t} + \mathrm{t_o}$, where n is the number of halve-wavelengths which fit into the length of $\mathrm{t} + \mathrm{t_o}$ and t_0 is the penetration depth into the finitely high potential walls by the electron wave function (with $\lambda = 2\pi/\mathrm{k}_\perp$ the equation above is reduced to Eq. (1)). The wave vectors $k_\perp$ can be determined from $k_\perp = \pi \times (n_2 - n_1)/(t_2 - t_1)$, where pairs t_1, n_1 and t_2, n_2 satisfy the quantisation condition equation (1) at the same energy [2]. $(t_2 - t_1)$ is known once the respective coverages and the thickness of one ML have been determined. The film coverages have been estimated from the RHEED intensity oscillations, Auger electron diffraction [19] and spectroscopically through AES and UPS [44]. The orientation of the Au film will now be determined in order to obtain the thickness of one ML.

We note that the Au lattice on Nb(100) has the same misfit as Ag on Nb(100) or Pd on W(100) [20,29]. XPD and RHEED show that the growth of Au on Nb(100) is, as expected, similar to that of Ag or Pd [20,29]. Figure 3 shows the background corrected anisotropy of the Au-4f-XPS signal as a function of the emitted (polar) angle (XPD) from a 14 ML thick Au film deposited at 150 K on a flat (1×1) Au terminated Nb(100) surface. Similar XPD diagrams were also obtained from Ag, Pd and Cu films grown on Nb(100). In XPD [23–26] strong peaks caused by forward focusing appear at an angle corresponding to the position of dense-packed atomic chains. In between them, there appears signal anisotropy caused by second order diffraction. The same rocking curves were also obtained if: (i) the films were annealed (up to 500 K), (ii) the deposition was carried out at 300 K, or (iii) the deposition was done on a sputter-rough Nb(100) surface. This indicates the same atomic short range order independently of the film roughness. Comparing the polar angle scans (Fig. 3) with those obtained from: (i) (111)-oriented Au [27], Cu or Ir [26]; (ii) (100)-oriented Au [27], Cu or Ag [26]; and (iii) (110)-oriented Cu samples [26], we get the best coincidence in the case of a (110)-oriented sample [26]. The XPD curve obtained for the $[110]_{\rm Nb}$ direction (peaks at $\theta = 0°$ and $\theta \sim 60°$ caused by forward focusing) (Fig. 3a) agrees well with the polar scan of the Cu(110) sample along the 55° displacement (the $\langle 211\rangle$ direction) of the [110] direction of the (110) surface (polar scan marked with 55° in Figure 5 of Han et al. [26]). This means that Au grows on the Nb(100) surface with its hexagonal densest-packed (111) layers perpendicular to the surface and along its [110] direction. A fcc stacking sequence (the natural phase of Au) of these densest-packed layers should lead to the fcc(110) orientation of the film. Indeed, if we compare the normal emission ARUPS spectra of thick Au films deposited on Nb(100) (Figs. 1, 2, 3) with those measured from (111) [21], (100) [21], or (110) [22] oriented fcc Au samples, the best coincidence is obtained for the fcc(110) orientation. Nevertheless, the polar scans of Figure 3 and also the curve marked

with 55° in Figure 5 of Han et al. [26] actually do not show this stacking sequence. They only show that hexagonal densest-packed atomic layers lie perpendicularly to the surface and along the $[110]_{Nb}$ azimuth in such a way that the surface normal and the [110] direction are aligned. This is an important result, since it shows that the confined direction (the surface normal direction) of the Au films deposited on (1×1)-terminated Nb(100), being along the [110]-direction, is not perpendicular to any surface of the bulk BZ, independently of the structure of the stacking sequence of the hexagonal densest layers (fcc, hcp, dhcp, ...) [43].

A close look at the rocking curves reveals that the peak in Figure 3a is located slightly before $\theta = 60°$, and that related to the fcc(110) orientation (curve marked with 55° in Fig. 5 of Han et al. [26]) slightly after $\theta = 60°$. The differences are more pronounced if the polar scans are done along the azimuth directions: 45° off the $[110]_{Nb}$ direction (Fig. 3b) and the $\langle 211\rangle$ direction (curve marked with 10° in Figure 5 of Han et al. [26]). The curve obtained from the (110)-oriented fcc film (curve marked with 10° in Figure 5 of Han et al. [26]) shows a weak peak at $\theta = 45°$, whereas that obtained in the [100] direction of the Nb(100) surface shows a peak at a larger polar angle of $\theta \sim 49°$. These differences can be attributed to a stacking sequence which is different from the fcc one. Indeed, the polar scans of Figure 3a coincide even better with those obtained from films with an hcp-stacking sequence [28]: Gazzadi and Valeri [28] have also measured a strong peak situated slightly below $\theta = 60°$ in thick $(11\bar{2}0)$-oriented hcp Co films grown on Fe(100).

RHEED from flat Au films shows an almost square 2-dimensional (2D) unit cell of the hexagonal $(11\bar{2}0)$ orientation which agrees well with that of the Nb(100) surface [29]. In [29] we showed that RHEED transmission can clearly distinguish between an hcp and fcc epitaxy. In order to obtain the relevant RHEED transmission patterns we deposited Au on a clean, mildly sputtered Nb(100) surface, where ARUPS and XPD show the same short range order as in the case of Au deposited on a flat Nb(100) surface. The obtained transmission pattern is shown in Figure 4a. We have obtained similar centred RHEED transmission patterns from Cu and Co films deposited on W(100) [29], and demonstrated that such patterns can only be produced by a $(11\bar{2}0)$-oriented hexagonal stacking sequence and not by a fcc one [29]. This conclusion has recently been confirmed by Jona et al. [30], who showed on the grounds of a LEED-IV structure analysis that Cu films deposited on W(100) possess a $(11\bar{2}0)$-oriented hcp structure. Similarly, an X-ray diffraction (XRD) study of Co films deposited on Mo(100) [35] and on (100)-oriented Cr buffer layers [32–35], which exhibit similar centred RHEED transmission patterns, proved the existence of the $(11\bar{2}0)$-oriented hcp phase of Co. Wu et al. [36] performed transmission electron diffraction (TED) (which probes the bulk and not the surface) on Co films deposited on GaAs(100), finding that the films have the $(11\bar{2}0)$ oriented hcp phase, and thus confirming previous TED results of Gu et al. [37]. A similar result was subsequently

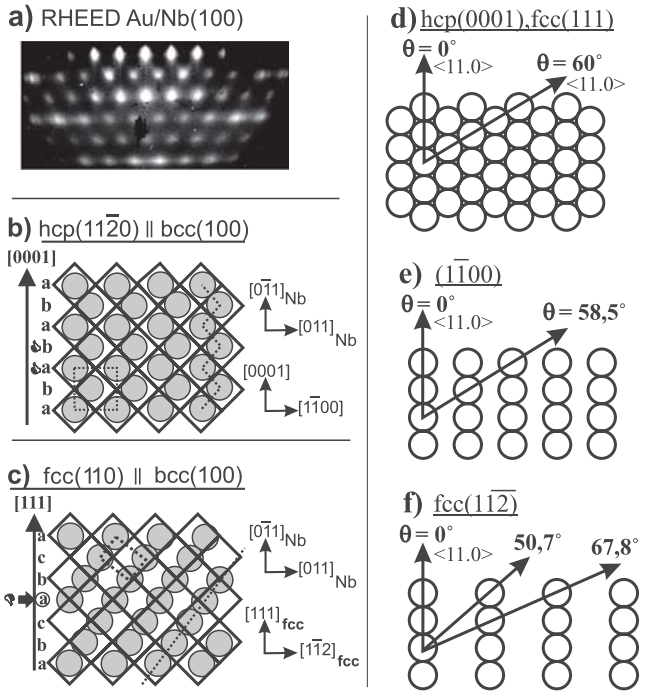

Fig. 4. a) RHEED pattern of a 20 ML thick Au film deposited on Nb(100) in the $[011]_{Nb}$ direction. b, c) Schematic illustration of the $(11\bar{2}0)$-oriented hcp (b) and (110) oriented fcc (c) epitaxy of Au on Nb(100). Au atoms are represented by grey circles and Nb atoms are situated at the corners of the sketched quadratic (100) lattice. In metallic epitaxy the hollow sites on the Nb(100) surface (the square centres) are the energetically most favourable, whereas the on-top positions (the square corners) are the most unfavourable adsorption sites. d, e, f) Graphs related to the XPD measurements: (111) (panel (d)), and $(1\bar{1}2)$ cut (f) through an fcc and (0001) (d) and $(1\bar{1}00)$ cut (e) through an hcp crystal, showing atomic dense-packed directions.

obtained in TED from Co films deposited on Au(100) by Oikawa et al. [38] and confirmed by Bayle-Guillemaud and Thibault [39], who performed an atomic resolved electron microscopy study on these films. Using atomic resolutions for the surface and for cross-sections through the films, they found the $(11\bar{2}0)$ oriented hcp phase [39]. These results clearly demonstrate that the RHEED pattern of Figure 4a is produced by Au films which have the $(11\bar{2}0)$ oriented phase (hcp).

In this orientation the hexagonal dense-packed (0001) atomic plains lie perpendicularly to the Nb(100) surface. The stacking sequence axis ([0001]) is positioned in the Nb(100) surface showing a very good fit to the $\langle 011\rangle$ direction of this surface (Fig. 4b) [29]. A much better fit of the hcp stacking sequence to the Nb(100) surface (Fig. 4b) than of the fcc sequence (Fig. 4c) explains lack of re-orientation of up to 100 ML thick Au films to the natural fcc structure. After a mild annealing (up to 500 K) of thick Au films, RHEED shows some evidence of a double-hcp stacking. Thus, the orientation relationship of Au on Nb(100) is: $Au(11\bar{2}0)[0001] \parallel Nb(100)\langle 011\rangle$, with the $[11\bar{2}0]$ direction being perpendicular to the surface. Consequently, the confined direction ([110]) is not

perpendicular to any surface of the bulk BZ, not even for the concurring fcc(110) orientation. In contrast to the Nb(100) surface, which has four-fold symmetry, the $(11\bar{2}0)_{\mathrm{Au}}$ surface has only two-fold symmetry. Although the orthogonal $[011]_{\mathrm{Nb}}$- and $[0\bar{1}1]_{\mathrm{Nb}}$-directions of the Nb(100) surface are equivalent, the orthogonal directions $[0001]_{\mathrm{Au}}$ and $[1\bar{1}00]_{\mathrm{Au}}$ are not. Therefore, Au grows on Nb(100) in two orthogonal domains. One with $[0001]_{\mathrm{Au}} \parallel [011]_{\mathrm{Nb}}$ and $[1\bar{1}00]_{\mathrm{Au}} \parallel [0\bar{1}1]_{\mathrm{Nb}}$ and the other with $[0001]_{\mathrm{Au}} \parallel [0\bar{1}1]_{\mathrm{Nb}}$ and $[1\bar{1}00]_{\mathrm{Au}} \parallel [011]_{\mathrm{Nb}}$ [29]. In analogy, if the stacking sequence were fcc, the fcc(110)-orientation would also lead to an Au growth on Nb(100) in two orthogonal domains: one with $[111]_{\mathrm{Au}} \parallel [011]_{\mathrm{Nb}}$ and $[11\bar{2}]_{\mathrm{Au}} \parallel [0\bar{1}1]_{\mathrm{Nb}}$ and the other with $[111]_{\mathrm{Au}} \parallel [0\bar{1}1]_{\mathrm{Nb}}$ and $[11\bar{2}]_{\mathrm{Au}} \parallel [011]_{\mathrm{Nb}}$ [29].

These two domains explain the differences mentioned above in XPD from Au layers on Nb(100) in comparison to the polar scans from (110)-oriented fcc samples. A polar scan along the [110] azimuth of the Nb(100) surface scans the hexagonal densest-packed atomic planes ((0001) or (111)): the $(1\bar{1}00)$ and {211} plane for an hcp and fcc stacking sequence, respectively. The scan along the normal direction ($\theta = 0^{\mathrm{o}}$) always produces a strong peak in XPD, because for all scanned planes, the dense-packed $\langle 110 \rangle$ atomic chain lies perpendicularly to the surface. Beside this strong normal emission peak, the scan along (0001) or (111) produces a peak at $\theta = 60°$ due to the forward focusing along the dense-packed $\langle 110 \rangle$ atomic chain situated at $\theta = 60^{\mathrm{o}}$ off the surface normal direction (Fig. 4d). The scans along $(1\bar{1}00)$ and {211} produce peaks at $\theta = 58.5^{\mathrm{o}}$ (Fig. 4e) and $\theta = 67.8^{\mathrm{o}}$ (Fig. 4f), respectively. Thus, for an hcp stacking sequence a superposition of peaks situated at $\theta = 60^{\mathrm{o}}$ and $\theta = 58.5^{\mathrm{o}}$ would result in a peak in XPD situated slightly before $\theta = 60^{\mathrm{o}}$, like that of (Fig. 3a), and the one obtained from $(11\bar{2}0)$-oriented hcp Co films [28]. An fcc stacking sequence would lead to a superposition of the peaks at $\theta = 60^{\mathrm{o}}$ and $\theta = 67.8^{\mathrm{o}}$ producing a peak shifted slightly toward polar angles larger than 60°. The both stacking sequences (fcc and hcp) do not posses dense-packed atomic chains in planes positioned at the azimuth angle of $\phi = 45^{\mathrm{o}}$ (displacement in the surface plane) relative to the stacking planes, which explains the low intensity of the peaks at polar angles different from zero in comparison to the normal emission peak in the XPD curve measured along the [100] direction of the Nb(100) surface (see Fig. 3b). The normal emission peak occurs with the same high intensity independently of the scanned azimuth direction, because it is caused by the forward focusing of the emitted photoelectrons along the dense-packed [11.0] atomic chain which is normal to the surface.

Knowing that the confined direction of the Au film is $[11\bar{2}0]$, we can now determine the thickness d of the Au monolayer: $d = a/2$, where a is the nearest-neighbour distance in bulk Au. In order to calculate the values of $k_\perp$ from the QSE data we still need to assign quantum numbers n to the QSE maxima of Figure 1a. Inspecting this figure, we observe that there are four families of maxima marked with natural numbers 1–4. The assumption that one set of maxima corresponds to one quantum number n allows us to follow the evolution of the quantum states (maxima) with the thickness and of course with the energy (Fig. 5a). $E(k_\perp)$ determined on the grounds of the equation $k_\perp = \pi \times (n_2 - n_1)/(t_2 - t_1)$ are marked with squares in Figure 5b.

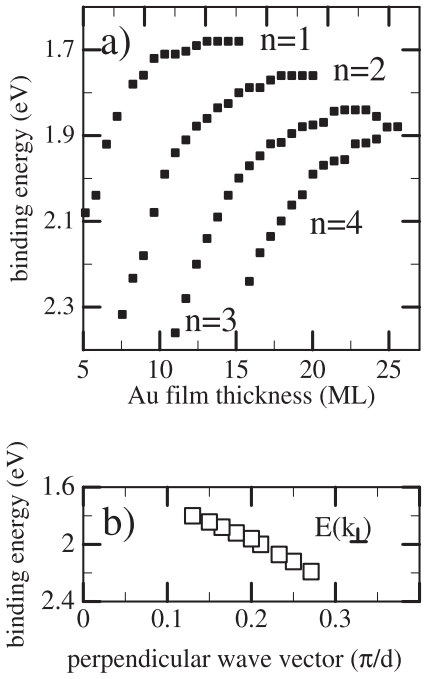

Fig. 5. a) Energy positions of the QSE features shown in Figure 1 as a function of the Au coverage. b) $E(k_\perp)$ values determined from the QSE shown in panel (a).

3.3 Comparison of the determined $E(k_\perp)$ with the bulk band structure

We will now explain the observed QSE in terms of the bulk band structure of Au in the confined direction, which is given in Figure 7. As it can be seen in Figures 6, 7, vector $k = \pi/d$, in terms of which the values of $k_\perp$ have been given, lies at point M, which has inversion symmetry. Point M, in turn, lies exactly between two Γ points in the direction $\langle 11\bar{2}0 \rangle$ of the bulk BZ which has the periodicity of $k = 2\pi/d$ in this direction. Thus, the end of vector $k = \pi/d$ lies outside of the first bulk BZ and not at the BZ boundary (point K). This is different from the QSE analysed thus far, where the determination of the $E(k_\perp)$ values always made use of $k = \pi/d$ situated at the BZ boundary [6]. Our experimentally determined values of $E(k_\perp)$ are marked with squares in the long left panel of Figure 7. We observe that no agreement with the bulk band structure can be obtained, unless the $E(k_\perp)$ values (encircled with the oval lines in Fig. 7) are referred to point M and not to point Γ of the bulk BZ. As already mentioned in the Introduction, two models of QSE have been designed to deal with such discrepancies. In the "envelope model" the wave vectors $k_\perp$ of QWS are related to the wave vectors $\widetilde{k_\perp}$ obtained from quantum size

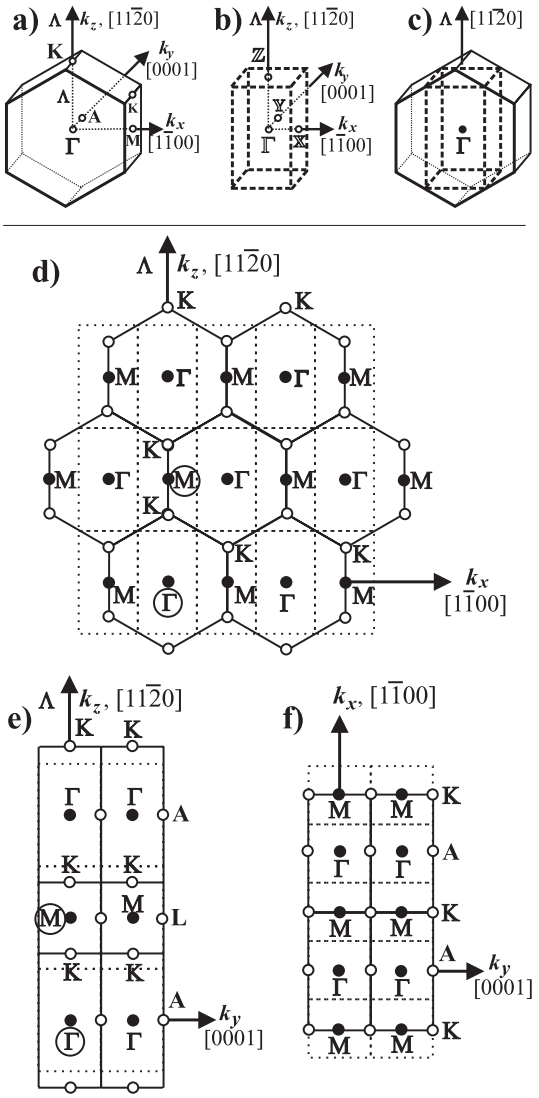

Fig. 6. a) Hexagonal bulk BZ. b) Orthorhombic LSA-BZ of (110) oriented films. c) Position of the LSA-BZ inside the bulk BZ. d, e, f) ($k_y = 0$)-plane (d), ($k_x = 0$)-plane (e) and ($k_z = 0$)-plane (f) in the repeated zone scheme. LSA-BZ is drawn with dotted lines. Only some symmetry points of the bulk-BZ are represented in the figure.

oscillations by the formula $k_\perp = \pi/d - \widetilde{k_\perp}$ [6]. This justifies the change of the reference point from point Γ to point M which we have had to perform above to get agreement between the measured energies and the bulk band structure. The "reduced quantum number model" proposes a different assignment of quantum numbers n to the observed QSE maxima. It introduces a reduced quantum number $\nu = N - n$, where N is the number of monolayers. Indeed, if the reduced numbers ν instead of n are assigned to the observed QSE maxima, the measured QSE energies agree with the bulk band structure. The two models explain all the QSE observed so far. There are, however, QSE states, like those in thin Mg [46] and Gd [47] films, that can be explained without referring to those models. A question, thus, arises why the application of the two models is necessary for the explanation of the observed QSE energies in terms of the respective bulk band structures only in some cases, while other cases can be explained without these models.

The considerations above show that although the two models bring about agreement between the measured values and the bulk band structure (Fig. 7) the respective $k_\perp$ lie outside of the first BZ. The part of the k-space that is really physically significant is the first BZ, since it contains all the irreducible bulk states [45]. Thus, it must also be possible to transform the states encircled with the oval line in the long l.h.s. panel of Figure 7 back into the first BZ, using the symmetry of the reciprocal space. The bulk states corresponding to these QWS are situated on the surface of the first bulk BZ between points K and M (Fig. 6). Thus, their wave vectors do not lie in the confined direction as required by the quantum well. Obviously, the procedure of finding equivalent k points in the first BZ cannot be applied to the system under investigation (Au film) since the confined direction is unique in this case and, consequently, there are no symmetry operations which could transform it into another equivalent direction in the first BZ. This clearly shows that the conventional first bulk BZ is not adequate for the explanation of the QWS. To remedy the situation, we will now take into account the symmetry of the film to construct what will be further referred to as the layer symmetry adapted Brillouin zone (LSA-BZ).

In contrast to bulk hcp Au, an [11$\bar{2}$0] oriented Au film has only 2 dimensional (2D) translational symmetry extending to infinity (in the plane parallel to the surface of the layer) with a rectangular P (RP) Bravais lattice [42]. Consequently its first BZ is also 2D, with the two basis vectors of the reciprocal lattice $|\mathbf{b_1}| = 1.25$ Å^{-1}, $|\mathbf{b_2}| = 1.33$ Å^{-1} lying in the directions [1$\bar{1}$00], [0001], respectively. Since we would like to explain the QWS in terms of the bulk band structure and are not interested in surface states, we can assume that the system has translational symmetry also in the direction perpendicular to the surface of the layer with the Born - von Karman periodicity condition $\{\mathbf{1}|l \cdot (2\mathbf{d})\} = \{\mathbf{1}|\mathbf{0}\}$, where $\mathbf{1}$ is the identity element, l is a natural number and $\vec{d}$ is a vector perpendicular to the surface of the layer, whose length is equal to the ML thickness ($2\mathbf{d}$ gives the translational periodicity in the confinement direction). This gives a 3-dimensional BZ, which is a rectangular parallelepiped in the k-space, its base being the 2D BZ of the Au film and its height π/d (see Fig. 6b, c).

It can be seen in Figure 6 that the $k_\parallel$ periodicity in the [1$\bar{1}$00] direction is in the LSA-BZ (drawn with dashed lines) of (110)-oriented hexagonal films two times smaller than in the hexagonal bulk BZ. On the other hand, the periodicity in the [0001] direction is the same in the LSA-BZ as in the bulk BZ. Similar differences also occur for films with the fcc crystal structure. Panel (a) of Figure 8 shows the bulk BZ of an fcc crystal and inside it, drawn with dashed lines, the LSA-BZ of (001)-oriented fcc films if [100] is the confined direction. This BZ is also the LSA-BZ of (01$\bar{1}$)-oriented fcc-films if the [$\bar{1}$10] is the confined

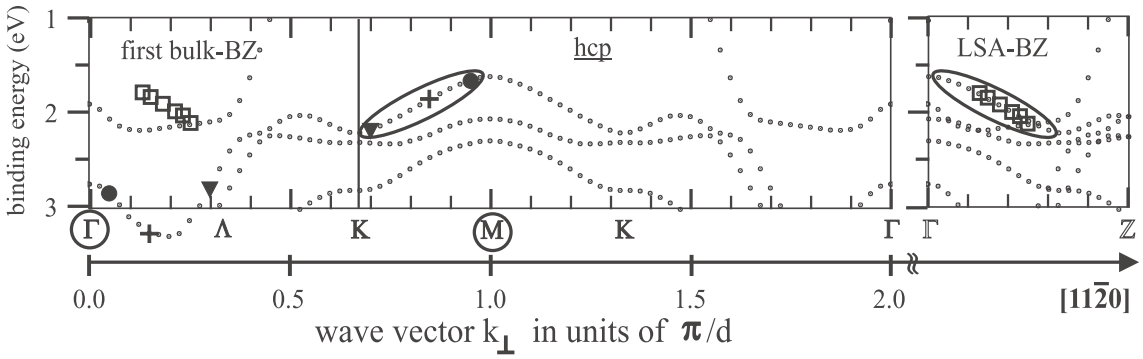

Fig. 7. Bulk band structure ($E(k_\perp)$) of hcp Au in the [11$\bar{2}$0]-direction given in the bulk BZ (left long panel) and in the LSA-BZ (right short panel).

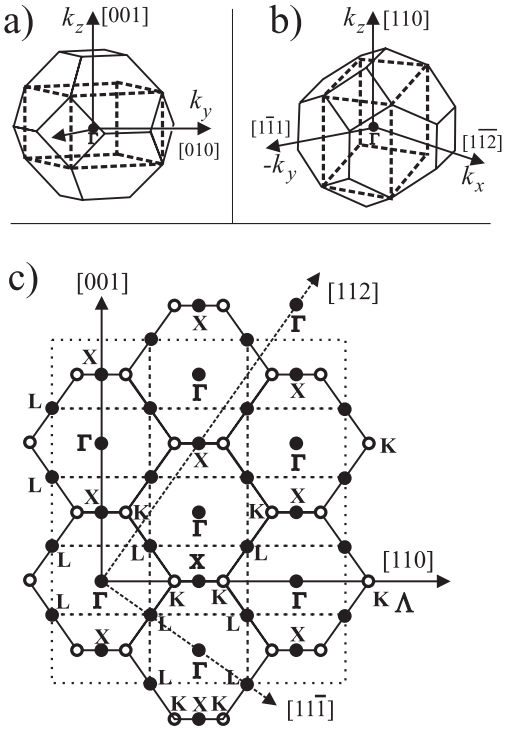

Fig. 8. a) LSA-BZ of (001)-oriented fcc films (drawn with dashed lines) positioned inside the fcc bulk-BZ. k_x and k_y axes are parallel to the ⟨100⟩-directions, respectively, whereas k_z direction is parallel to the surface normal direction of (001)-oriented fcc films. Basis planes of this tetragonal LSA-BZ lie perpendicularly to the [001] (k_z)-direction, whereas two side planes are perpendicular to the ⟨110⟩- (ΓK) directions. b) The same as panel (a), but now the [110]-, [111]- and [112]- crystal axes are parallel to the k_z, k_y and k_x axes of the Cartesian coordinate system. If again the k_z direction (now [110]) is chosen to be the confined one, the parallelogram drawn with dashed lines in panel (b) is the LSA-BZ of (110)-oriented fcc films, whose shape is identical to that of (001)-oriented fcc-films. The [110] direction is perpendicular to the basis planes of the LSA-BZ, but [110] is not perpendicular to any planes of the fcc bulk BZ. c) Cut through the BZ of panel (a) or (b), which contains the Γ points of the BZ and the [001]- and [110]-directions. The cut through LSA-BZ is again drawn with dashed lines. Only some points of the fcc-bulk BZ are represented in the figure.

direction. The periodicity in the [001]- and [110]-direction of the $k_\parallel$-plane is in the LSA-BZ two times smaller than in the bulk BZ, whereas the $k_\parallel$ periodicity in the [111] direction is in the LSA-BZ the same as in the bulk BZ. Since the periodicity of the 2D BZ of the film is different from the $k_\parallel$ periodicity of the bulk BZ, the LSA-BZ can be verified by the experimental determination of the $k_\parallel$ dependence of the QWS.

3.4 Experimental determination of the $k_\parallel$-periodicity of QWS

ARUPS is a powerful technique for the determination of $E(k_\parallel)$ bands because the $k_\parallel$ component of the wave vector is conserved during the photoelectron emission process [41]. The parallel components of the wave vector of the detected electrons and of the excited (final) band state are equal, and in the case of a direct (k-conserving) transition, equal to the parallel component of the initial state. The $k_\parallel$ values of the initial emission state can be calculated from [41]

$$k_\parallel = \frac{1}{\hbar}\sqrt{2m_e E_{kin}} \cdot \sin\theta = \frac{1}{\hbar}\sqrt{2m_e(h\nu - \Phi - |E_B|)} \cdot \sin\theta \tag{2}$$

where θ is the emission angle, E_{kin} – the kinetic energy of the emitted photoelectron, Φ – the work function of the film, E_B – the binding energy of the initial state and $h\nu$ – the energy of the absorbed photon. Thus, $E(k_\parallel)$ can be obtained from off-normal ARUPS measurements and, subsequently, it can be used to determine the $k_\parallel$ periodicity of the band states.

The off-normal ARUPS emission from QWS have been measured in thin (111) [2,12] and (100) [3] oriented Ag films, (111)-oriented Al films [12,13], (0001)-oriented Mg films [12] and in thin (100)-oriented Cu films [14]. However, the $k_\parallel$-periodicity of the QWS was not determined on the grounds of these measurements due to the *sp* character of the observed QWS. In all those cases the *sp*-$E(k_\parallel)$ bands cut the Fermi level leaving the BZ boundaries unoccupied and, therefore, not accessible to ARUPS.

In contrast, our calculations show that the QWS shown in Figure 7 (encircled with oval lines) are of *d* type. Since

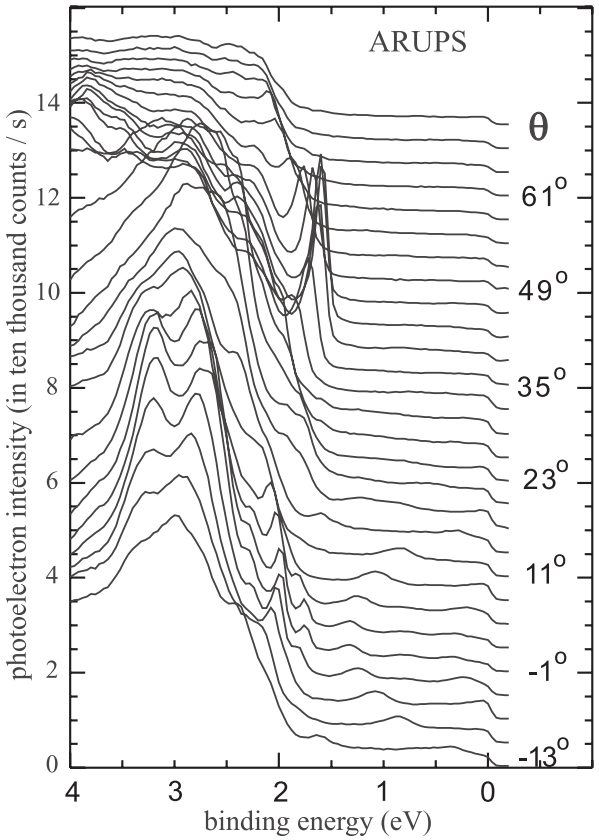

Fig. 9. Off-normal ARUPS spectra of an 11 ML thick Au film deposited on Nb(100). The Au film was deposited at 150 K, and subsequently annealed to 500 K (for 1 minute), which improved its long range order. The emission angle was changed in the $[011]_{\mathrm{Nb}}$ direction of the Nb(100) surface.

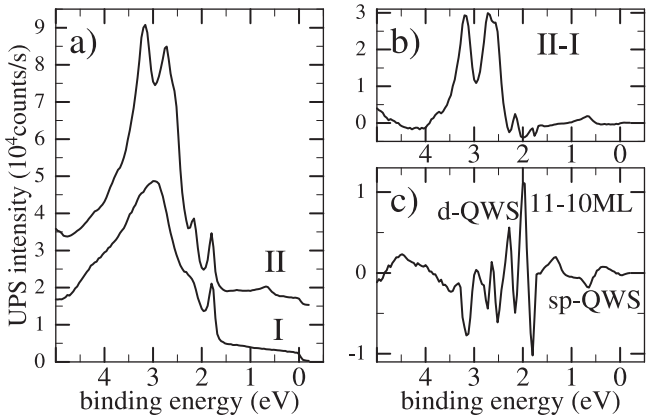

Fig. 10. a) Normal emission UPS spectra (marked with I) of a non-annealed 10 ML thick Au film deposited on Nb(100) at 150 K and of the same film, subsequently annealed at 500 K for 1 minute (spectra marked with II). For a better representation, 16 000 counts were added to the intensity of the UPS spectrum of the annealed film. b) Difference (annealed – non-annealed) between the UPS spectra of panel (a) (II-I). c) Difference between the UPS spectra obtained from an 11 ML thick and a 10 ML thick Au film. The Au films were deposited first at 150 K on Nb(100) and subsequently annealed for 1 min. at 500 K.

the d bands in Au are fully occupied, it is expected that the $E(k_{\|})$ bands do not cross the Fermi level and, consequently, can be probed with ARUPS. The sought for $k_{\|}$ periodicity of the QWS can, thus, be determined from the measured $E(k_{\|})$ dependence of the d-type QWS. Figure 9 shows ARUPS spectra of an 11 ML thick Au film grown on Nb(100) measured at different emission angles. The Au film was annealed for 1 minute at 500 K, which led to an improved long range order, reducing the background in the UPS spectra and sharpening the UPS peaks. As a consequence, weak peaks from a strongly dispersed *s-p* QWS appeared between 1.3 and 0 eV (Fig. 9), which can also be observed in Figure 10 at the energy of 0.65 eV. The spectra marked with (I) in Figure 10a were obtained from a non-annealed 10 ML thick Au film, and those marked with (II) from the film annealed at 500 K for 1 minute. Such annealing smooths out films like those of Pd or Ag deposited at 150 K on W(100) [29] or on Nb(100) [44]. Using STM, Smith et al. [40] have explained this process in the case of Ag films deposited on GaAs. Deposition of a critical thickness at low temperatures leads to the formation of a dense nanocluster film. Upon annealing its atoms rearrange themselves into an atomic flat film [40].

However, Au on Nb(100) does not exhibit such a behaviour. The energy position of the QSE peaks between 1.8 eV and 2.3 eV (Fig. 10a) are not affected by the annealing, which shows that this process does not affect the thickness distribution in the investigated region of the Au film. Thus, it can be concluded that the Au films deposited on Nb(100) at 150 K are already flat, which is confirmed by the occurrence of the pronounced QSE in the non-annealed Au films (Fig. 1). Still, the annealing affects the films by improving their long-range order, which is evidenced by RHEED. At the same time the short-range order of the films remains unchanged, since the XPD spectra before and after the annealing are the same. The improved long range order reduces the background in UPS and sharpens the UPS peaks considerably, especially in the energy range between 2.5 eV and 3.5 eV, which can also be seen in the difference spectra between the annealed and non-annealed Au film (Fig. 10b). The minima and maxima occurring in the difference spectra between an annealed 11 ML (Fig. 9) and an annealed 10 ML Au film (Fig. 10a) show that the energy positions of the peaks between 3.5 eV and the Fermi level change with the film thickness. As already mentioned, this behaviour can be explained by the emission from the QWS whose wave vector in the confined direction changes with the film thickness. In Figure 10c the energy difference between the consecutive extrema positioned between 3.5 eV and 1.7 eV is smaller than between those situated in the range 1.5 eV and 0 eV. These observations suggest that the QSE maxima between 3.5 eV and 1.7 eV originate from d states, whereas those between 1.5 eV and 0 eV from *sp* states, because *sp* states have, in general, stronger energy dispersion than d states. Our calculations show that the strong QSE emission between 3.5 eV and 1.7 eV occurs from the QWS with d band character whose band dispersion ends at 1.6 eV, where M point of the bulk BZ (Fig. 7)

is reached. On the other hand, the weaker QSE emission in between 1.5 eV and the Fermi energy (Fig. 10c) originates from a *sp* band with a stronger band dispersion intersecting the Fermi level. In the normal emission spectra ($\theta \sim 0°$) of Figure 9, the weak QSE peaks originating from the *sp* band are located at 1.3 eV, 0.7 eV and 0.3 eV. In contrast to the stronger emission from *d* bands, the emission from the *s-p* QWS is too weak in the case of the non-annealed Au films to be distinguished in the form of peaks from the structureless background emission (Figs. 1, 10a). Despite the poor long range order, the observation of QWS between 2.3 eV and 1.7 eV in non-annealed films confirms the *d* character of these states (*d* states of noble metals have much stronger photo-electron emission yield than *sp*-states, and thus the emission from these states occurs even when there is no long-range order). This character is further confirmed by the behaviour of the $E(k_\parallel)$ bands related to these states, which do not cross the Fermi level, dispersing to binding energies lower than 1.5 eV in the whole $k_\parallel$ region. In the off-normal ARUPS spectra of Figure 9 the emission angle (θ) was changed along the $[011]_{\mathrm{Nb}}$ direction of the Nb(100) surface. Taking into account the epitaxial relation of Au on Nb(100) and the fact that ARUPS averages over the investigated part of the sample, the measured $E(k_\parallel)$ is a lateral average over the $[0001]_{\mathrm{Au}}$ and $[1\bar{1}00]_{\mathrm{Au}}$ directions for the hcp and dhcp, and over the [111] and $[1\overline{12}]$ directions for the fcc stacking sequence of Au. Panel (a) of Figure 11 shows the dependence of the UPS spectra on the emission angle. The strength of the UPS emission is indicated as follows: big black dots correspond to strong UPS peaks, big non-filled circles correspond to smaller but well distinguishable UPS peaks or to shoulders of high intensity, whereas the small dots correspond to peaks or shoulders of low intensity. The $k_\parallel$ values of the initial emission states can be calculated from equation (2). The resulting $E(k_\parallel)$ dependence of the QSE maxima occurring in the Au film is presented in Figure 11b. The states which correspond to $E(k_\parallel = 0)$ lie in panel (a) on the vertical straight line, but those which correspond to $E(k_\parallel = 1.26$ Å$^{-1})$ lie on the curved line marked with an arrow. This shows, that except for the normal emission spectra ($\theta \simeq 0$), the peaks in the off-normal spectra correspond to different $k_\parallel$ values. It can be observed that the $k_\parallel$ values of the emitted states increase with the increasing value of the emission angle.

Panel (c) of Figure 11 shows the $E(k_\parallel)$ dependence of the QWS plotted without indicating their UPS-emission strength. The dispersions seems to be symmetric about $k_\parallel = 0$ Å^{-1}, $k_\parallel = 0.62$ Å^{-1} and $k_\parallel = 1.25$ Å^{-1}. The behaviour of the dispersion around $k_\parallel = 0$ Å^{-1} is identical with that around $k_\parallel = 1.25$ Å^{-1}, as if the $\Gamma_\parallel$ point was reached again there. Although the dispersion behaviour is similar around these points, the energy positions of the corresponding states are slightly different. For example, the lowest lying state in Figure 11c has at $k_\parallel = 0$ Å^{-1} the energy of $\simeq$1.75 eV, whereas the state with the same dispersion has at $k_\parallel = 1.25$ Å^{-1} the energy of $\simeq$1.60 eV. We suspect that this small discrepancy in energy has two reasons: one is a ground state effect related to the confinement of the film states, and the other – a final state effect in photo-electron spectroscopy.

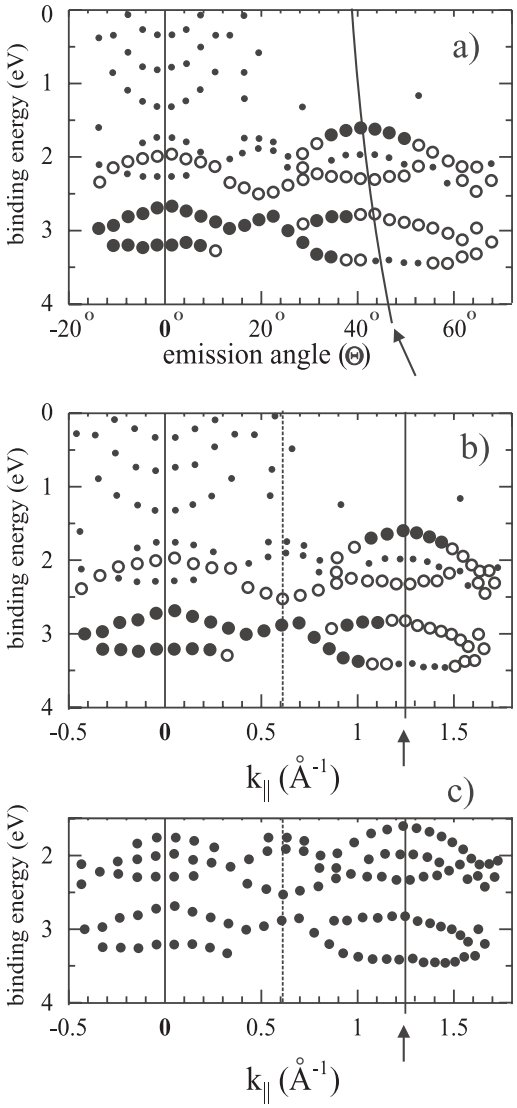

Fig. 11. a) Energy positions of the ARUPS features (intensity peaks and shoulders) of an 11 ML thick Au film as a function of the emission angle (θ). States marked with black filled circles correspond to peaks with high UPS emission. States marked with non-filled circles correspond to peaks of lower UPS emission and to shoulders. States marked with small circles correspond to peaks with very low UPS emission or only to small shoulders. b) $E(k_\parallel)$ dependence of the QSE maxima shown in (a). The vertical thick lines show the $E(k_\parallel = 0)$ and $E(k_\parallel = 1.26$ Å$^{-1})$ states. The states which correspond to $E(k_\parallel = 0)$ lie in panel (a) also on the vertical straight line and those which correspond to $E(k_\parallel = 1.26$ Å$^{-1})$ lie on the curved line marked with the arrow. c) $E(k_\parallel)$ dependence without the photoemission intensity indicated.

The first effect occurs, because the quantised vector $k_\perp$ changes with in-plane momentum $k_\parallel$ [14], due to the dependence of the phase shift of QSE on $k_\parallel$ at the film-substrate boundary. In the case of an idealised quantum well with infinitely high potential walls, the $k_\perp$ values are determined only by the thickness of the well (t) according

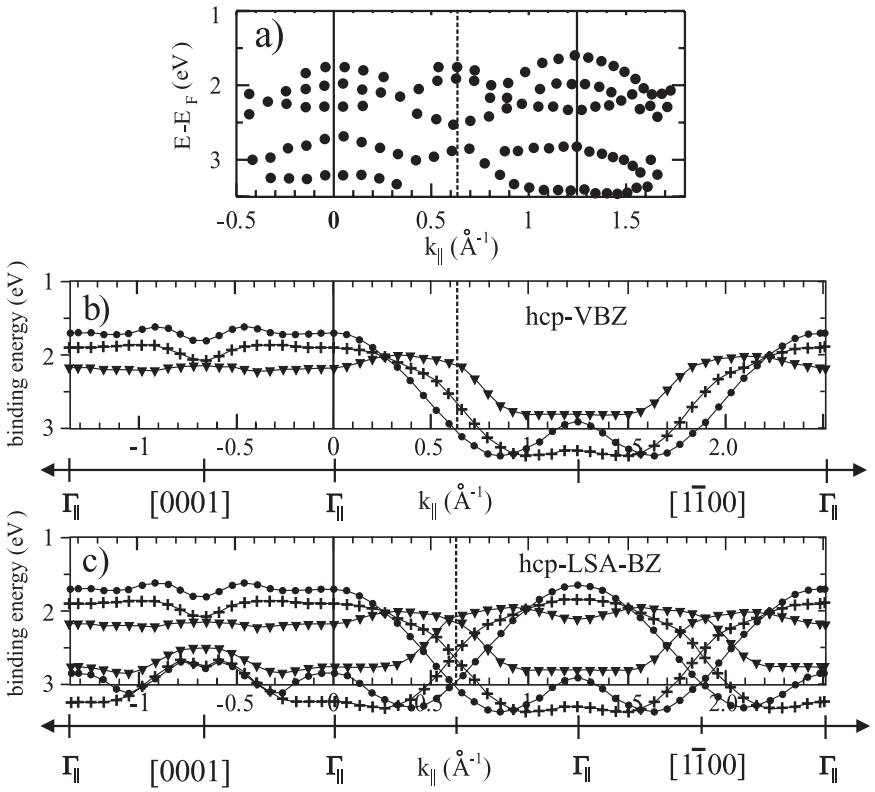

Fig. 12. a) The experimentally determined $E(k_\parallel)$-dependence of QWS in a 11 ML thick Au film deposited on Nb(100) (Figs. 9, 11). b, c) The $E(k_\parallel)$ ($E(k_{xy})$) dependence of the $E(k_\perp)$-states marked in Figure 7 with a circle, a cross, and a triangle given in the bulk BZ (b) and in the LSA-BZ (c).

to the quantisation condition ($2k_\perp \cdot t = 2n\pi$) and, consequently, the $k_\perp$ values are independent on $k_\parallel$. However, for a real quantum well with finite potential walls, the quantisation condition is supplemented with the phase shift (Φ) at the film boundaries ($2k_\perp \cdot t + \Phi = 2n\pi$), because the electron wave penetrates the well walls. Thus, the phase shift depends on the energy and also on the coupling of the film and substrate states. The coupling strength depends on the energy and k-space topology of the band gap in the substrate, which, in turn, depends on $k_\parallel$. Consequently, the phase shift of the QWS on the film-substrate boundary depends on $k_\parallel$, and therefore, due to the quantisation condition ($2k_\perp \cdot t + \Phi = 2n\pi$), $k_\perp$ also depends on $k_\parallel$. Thus, in the case of a real quantum well, the $k_\perp$ values are depend on, beside thickness t, also $k_\parallel$. This was confirmed by Wu et al. [14] who measured with ARUPS the dependence of $k_\perp$ on $k_\parallel$ in QSE occurring in thin Cu films. This explains why the states discussed above have slightly different energies: their vectors $k_\parallel$ are different ($k_\parallel = 0$ Å^{-1} and $k_\parallel = 1.25$ Å^{-1}), and consequently their $k_\perp$ and, with it $E(k_\perp)$ are also different. Since the phase shift also depends on the energy, the magnitude of the energy discrepancy depends on the QWS energy.

The second reason for the energy discrepancy can be a final state effect, because the electronic structure of the ground state may be inaccessible with photo-electron spectroscopy [15]. Final state effects can be different at different $k_\parallel$-values, leading to UPS peaks at different energies for equivalent states having different $k_\parallel$ values. We suspect that both effects, the final state effect and the QSE caused dependence of $k_\perp$ on $k_\parallel$ are responsible for the small energy discrepancy of the states with the identical dispersion shown in Figure 11.

In this context, the $E(k_\parallel)$ dependence of Figures 11b, c indicates that the $k_\parallel$ periodicity of the QSE states is $k_\parallel \simeq 1.25$ Å^{-1}. This periodicity is the same as that of the 2D BZ of the (11$\bar{2}$0) oriented Au film in the [1$\bar{1}$00] direction and two times smaller than the respective periodicity of the hcp bulk BZ in the same direction. It is also consistent, within the experimental error, with the periodicity of the 2D BZ in the [0001] direction, which is the same as that of the hcp bulk BZ in this direction. Thus, the obtained results confirm the proposed shape of the LSA-BZ in the $k_{x,y}$ plane.

3.5 Comparison of the E(k$_\parallel$) dependence of QWS with that of bulk Bloch states

The $E(k_\parallel)$ dependence of the bulk Bloch states of the 11 ML thick Au film is given in the bulk BZ in Figure 12b and in the LSA-BZ in Figure 12c. According to the quantisation condition $k_\perp(E)\cdot t + \Phi(E) = n\pi$, the layer has in the confined direction the wave vectors $k_\perp(E) = n\pi/(11d) - \Phi(E)/(11d)$. If the phase factor Φ was 0, the wave vectors

would be given by $k_\perp = n\pi/(11d)$, which for $n = 11, 10, 9$ gives the values $k_\perp = 11\pi/(11d)$, $k_\perp = 10\pi/11d$ and $k_\perp(E) = 9\pi/(11d)$. The UPS maxima related to QSE in the 11 ML thick Au-film occur in normal emission ($\theta \simeq 0$, $k_\parallel \simeq 0$) at 1.7 eV, 1.95 eV and 2.25 eV. The states with these energies have in the bulk band structure (Fig. 7) the following values of $k_\perp$: $10.45\pi/(11d)$, $9.35\pi/11d$ and $8.25\pi/(11d)$. Thus, the phase shifts for those states are $\Phi = 0.55\pi$, $\Phi = 0.65\pi$, and $\Phi = 0.75\pi$, respectively. In the bulk band structure (Fig. 7) the band states (1.70 eV, $k_\perp = 10.45\pi/(11d)$), (1.95 eV, $k_\perp = 9.35\pi/(11d)$), and (2.25 eV, $k_\perp = 8.25\pi/(11d)$) are marked with a black circle, a cross, and a black triangle, respectively. The $E(k_\parallel)$ dependence of these states is shown in Figure 12b, c in the $[0001](k_y)$ direction and the $[1\bar{1}00]$ (k_x) direction, where the bulk states with $k_\perp = 10.45\pi/d$, $k_\perp = 9.35\pi/d$, and $k_\perp = 9.35\pi/d$ are marked with circles, crosses and triangles, respectively. If the bulk band structure is given in the bulk BZ, then the states of Figure 12a which lie below 2.5 eV are missing in the [0001] direction. These states occur in the $[1\bar{1}00]$ direction but only at $k_\parallel = 1.25$ Å^{-1} and not at $k_\parallel = 0$, as is required by the experimental data of Figures 11, 12a. This clearly shows that the $k_\parallel = 1.25$ Å^{-1} periodicity is missing in the hcp bulk BZ. However, if the bulk band structure is given in the LSA-BZ, those states occur not only at $k_\parallel = 1.25$ Å^{-1} but also at $k_\parallel = 0$. In this case the measured $E(k_\parallel)$ dependence of the QWS agrees very well with the bulk band structure folded into the LSA-BZ. Thus, a question arises whether the $k_\perp$ periodicity of the QWS can also be obtained from their $E(k_\parallel)$ dependence.

In Figure 7 the states with $E_B \simeq 2.75$ eV, $E_B \simeq 2.85$ eV, and $E_B \simeq 3.25$ eV occur at $k_\perp = 2.75\pi/(11d)$, $k_\perp = 0.55\pi/(11d)$ and $k_\perp = 1.65\pi/(11d)$, respectively. Figures 12a, c show that the states with (1.95 eV, $k_\parallel = 0$) and (3.25 eV, $k_\parallel = 0$) correspond to the same value of $k_\perp$, although in the bulk BZ (Fig. 12b) they correspond to two different values of $k_\perp$: $9.35\pi/d$ and $1.65\pi/(11d)$, respectively. The same can also be said of the pairs of states which at $k_\parallel = 0$ have the energies of 1.7 eV, 2.85 eV and 2.25 eV, 2.75 eV. However, these pairs should have the same value of $k_\perp$ according to the experimentally determined $E(k_\parallel)$ dependence. This inconsistency can be removed if the periodicity in the confined direction is $k_\perp = \pi/d$, as in the LSA-BZ, and not $k_\perp = 2\pi/d$, as in the bulk BZ. This analysis demonstrates that the proposed LSA-BZ has the correct periodicity in the $[11\bar{2}0]$ direction.

4 Conclusion

We get strong d-type QSE in ARUPS from 5–26 ML thick $(11\bar{2}0)$ oriented Au films whose confined direction ([110]) is not perpendicular to any face of the bulk BZ. We subsequently show that: i) the $k_\perp$ values of the QWS determined with the help of the existing QSE models lie outside of the first bulk Brillouin zone. Because of the bulk translational symmetry (which extends to infinity in all directions) these states can be rearranged in the first bulk BZ but the corresponding Bloch states do not lie in the confined direction; ii) the measured $E(k_\parallel)$ dependence of these states gives a $k_\parallel$ periodicity which is consistent with the 2D periodicity of the Au layer but different from that of the bulk Brillouin zone. These results imply that the bulk BZ is not adequate for the explanation of the QWS. Instead, a Brillouin zone which conforms to the symmetry of the quantum well of the Au film (LSA-BZ) should be used. The LSA-BZ is a rectangular parallelepiped of hight π/d in the k-space, whose base is the 2D BZ related to the translational symmetry of the Au layer. Indeed, as it is shown in the right hand side panel of Figure 7, all the measured $E(k_\perp)$ values can now be explained in terms of the bulk band structure of hcp Au without the application of the envelope function and reduced quantum number models. It should be noted that the introduction of LSA-BZ leads to the folding of the bulk band structure around point $k_\perp = \pi/2d$ in the confined direction, which means that point $k_\perp = \pi/d$ of the bulk BZ corresponds to point $k_\perp = 0$ of the LSA-BZ. In contrast to the bulk Brillouin zones, the k points in the LSA-BZ always satisfy the equalities: $E(\text{-}k_\parallel) = E(+k_\parallel)$ and $E(\text{-}k_\perp) = E(+k_\perp)$. This is confirmed by the $E(k_\parallel)$ dependence of the QWS in thin Al(111) and Ag(111) layers [46] which shows that in the $[211]_{fcc}$ direction $E(\text{-}k_\parallel) = E(+k_\parallel)$, which is not satisfied in the fcc BZ. Besides, the LSA-BZ has the property that all the $k_\perp$ vectors are perpendicular to one of its faces. As a result, states with different values of $k_\parallel$ may still have the same $k_\perp$ components of their wave vectors, which is required for confined film states by the fact that the confinement is in the $k_\perp$ direction. This, in general, is not true for bulk BZs. Let us finally observe that in the case of thin [0001] oriented Mg [46] and Gd [47] films the bulk BZ is identical with the LSA-BZ and the QWS can be explained in terms of the bulk band structure given in the bulk BZ. This explains why the QSE models do not need to be applied in this case.

Discussions with Dr. L. Aballe on QSE in thin Al and Mg films and with Prof. L. Fritsche on QWS in thin films as well as on final state effects in photoelectron emission are thankfully acknowledged.

References

1. F.J. Himpsel, J.E. Ortega, G.J. Mankey, R.F. Willis, Adv. Phys. **47**, 511 (1998)
2. T.-C. Chiang, Surf. Sci. Rep. **39**, 181 (2000)
3. M. Milun, P. Pervan, D.P. Woodruff, Rep. Prog. Phys. **65**, 99 (2002)
4. Z.Q. Qiu, N.V. Smith, J. Phys. Condens. Matter **14**, R169 (2002)
5. R. Zdyb, E. Bauer, Phys. Rev. Lett. **88**, 166403 (2002)
6. J.E. Ortega, F.J. Himpsel, Phys. Rev. Lett. **69**, 844 (1992); J.E. Ortega, F.J. Himpsel, G.J. Mankey, R.F. Willis, Phys. Rev. B **47**, 1540 (1993)
7. N.V. Smith, N.B. Brookes, Y. Chang, P.D. Johnson, Phys. Rev. B **49**, 332 (1994)

8. R.K. Kawakami, E. Rotenberg, H. Choi, E. Escorcia-Aparicio, M. Bowen, J. Wolfe, E. Arenholz, Z. Zhang, N.V. Smith, Z. Qiu, Nature **398**, 132 (1999)
9. M. Steslicka et al., Surf. Sci. Rep. **47**, 93 (2002)
10. Two states whose wave vectors $k_\perp$ and $\widetilde{k_\perp}$ are given in the bulk-BZ are equivalent only if they can be reduced to one another by the periodicity of $2\pi/d$, which means that they are related to each other by $k_\perp = 2\pi/d - \widetilde{k_\perp}$
11. A. Beckmann, M. Klaua, K. Meinel, Phys. Rev. B **48**, 1844 (1993)
12. L. Aballe, thesis, Berlin, 2000
13. L. Aballe, C. Rogero, P. Kratzer, S. Gokhale, K. Horn, Phys. Rev. Lett. **86**, 5108 (2001)
14. Y.Z. Wu, C.Y. Won, E. Rotenberg, H.W. Zhao, F. Toyoma, N.V. Smith, Z.Q. Qiu, Phys. Rev. B **66**, 245418 (2002)
15. H. Eckardt, L. Fritsche, J. Phys. F **16**, 1731 (1986); L. Fritsche, Y.M. Gu, Phys. Rev. B **48**, 4250 (1993)
16. J.P. Perdew, K. Burke, M. Ernzerhof, Phys. Rev. Lett. **77**, 3865 (1996)
17. P. Blaha, K. Schwarz, J. Luitz, WIEN97, A Full Potential Linearised Augmented Plane Wave Package for Calculating Crystal Properties (Karlheinz Schwarz, Techn. Universität Wien, Austria), 1999, ISBN 3-9501031-0-4
18. E. Bauer, private communication
19. E. Hüger, K. Osuch, Europhys. Lett. **62**, 278 (2003)
20. E. Hüger, K. Osuch, Europhys. Lett. **63**, 90 (2003)
21. H.-G. Zimmer, A. Goldmann, Surf. Sci. **176**, 115 (1986)
22. P. Heiman, H. Neddermayer, H.F. Roloff, Phys. Rev. Lett. **37**, 775 (1976)
23. S.A. Chambers, Adv. Phys. **40**, 357 (1991)
24. D.P. Woodruff, A.M. Bradshaw, Rep. Prog. Phys. **57**, 1029 (1994); D.P. Woodruff, Surf. Sci. **299/300**, 183 (1994)
25. W.F. Egelhoff, Jr., in *Ultrathin magnetic structures I*, edited by J.A.C. Bland, B. Heinrich (Springer, Berlin, 1994), ISBN 3-540-57407-7
26. Z.-L. Han, S. Hardcastle, G.R. Harp, H. Li, X.-D. Wang, J. Zhang, B.P. Tonner, Surf. Sci. **258**, 313 (1991)
27. H. Wormeester, E. Hüger, E. Bauer, Phys. Rev. B **57**, 10120 (1998)
28. G.C. Gazzadi, S. Valeri, Europhys. Lett. **45**, 501 (1999)
29. E. Hüger, H. Wormeester, E. Bauer, Surf. Sci. **438**, 185 (1999); H. Wormeester, E. Hüger, E. Bauer, Phys. Rev. Lett. **77**, 1540 (1996)
30. F. Jona, X.Z. Ji, P.M. Marcus, Phys. Rev. B **68**, 075421 (2003)
31. *Reflection High-Energy Diffraction and Reflection Electron Imaging of Surfaces*, edited by P.K. Larson, P.J. Dobson, NATO ASI Series B **188** (Plenum, New York, 1988)
32. W. Donner, N. Metoki, A. Abromeit, H. Zabel, Phys. Rev. B **48**, 14745 (1993)
33. N. Metoki, W. Donner, H. Zabel, Phys. Rev. B **49**, 17351 (1994)
34. J.C.A. Huang, Y. Liou, H.L. Liu, Y.J. Wu, J. Crystal Growth **139**, 363 (1994)
35. Y. Liou, J.C.A. Huang, Y.D. Yao, C.H. Lee, K.T. Wu, C.L. Lu, S.Y. Liao, Y.Y. Chen, N.T. Liang, W.T. Yang, C.Y. Chen, B.C. Hu, J. Appl. Phys. **76**, 6516 (1994)
36. Y.Z. Wu, H.F. Ding, C. Jing, D. Wu, G.L. Liu, V. Gordon, G.S. Dong, X.F. Jin, S. Zhu, K. Sun, Phys. Rev. B **57**, 11935 (1998)
37. E. Gu, M. Gester, R.J. Hicken, C. Daboo, M. Tselepi, S.J. Gray, J.A.C. Bland, L.M. Brown, T. Thomson, P.C. Riedi, Phys. Rev. B **52**, 14704 (1995)
38. S. Oikawa, T. Kanno, S. Iwata, S. Tsunashima, J. Magn. Magn. Mat. **156**, 73 (1996)
39. P. Bayle-Guillemaud, J. Thibault, Phil. Mag. A **77**, 475 (1998)
40. A.R. Smith, K.-J. Chao, Q. Niu, C.-K. Shih, Science **273**, 226 (1996)
41. S. Hüfner, *Photoelectron Spectroscopy* (Springer, Berlin, 1995)
42. D.M. Hatch, H.D. Stokes, Phase Transitions **7**, 87 (1987)
43. C.J. Bradley, A.P. Cracknell, *The mathematical theory of symmetry in solids* (Clarendon Press, Oxford, 1972)
44. E. Hüger, K. Osuch, in preparation
45. S.L. Altmann, *Band theory of metals* (Pergamon Press, Oxford, New York, 1970)
46. L. Aballe, C. Rogero, K. Horn, Phys. Rev. B **65**, 125319 (2002)
47. O. Rader, A.M. Shikin, Phys. Rev. B **64**, 201406R (2001)
48. The fact that the observed states are of d type is not essential for the problems considered here. The d-type character of these states makes it only possible to determine their $k_\parallel$ periodicity from the measured $E(k_\parallel)$ dependence because the d bands in Au are fully occupied. Therefore, they do not cross the Fermi level, enabling us to determine with ARUPS (which only probes occupied bands) their $E(k_\parallel)$ dependence over the entire $k_\parallel$ region